Annals of Nuclear Energy 117 (2018) 194–201

Contents lists available at ScienceDirect

Annals of Nuclear Energy

journal homepage: www.elsevier.com/locate/anucene

Numerical investigation of the core outlet temperature fluctuation for the lead-based reactor

Lizhi Wang [a,b], Guowei Wu [a,*], Jin Wang [a], Ming Jin [a], Yong Song [a]

[a] Key Laboratory of Neutronics and Radiation Safety, Institute of Nuclear Energy Safety Technology, Chinese Academy of Sciences, Hefei, Anhui 230031, China
[b] University of Science and Technology of China, Hefei, Anhui 230027, China

ARTICLE INFO

Article history:
Received 22 November 2017
Received in revised form 5 March 2018
Accepted 14 March 2018
Available online 27 March 2018

Keywords:
Temperature fluctuation
Lead-based reactor
Core outlet

ABSTRACT

The temperature fluctuations induced by incomplete mixing of coolants with different temperature may cause thermal fatigue at the components of the lead-based reactor core outlet. Thus the accurate analysis of the phenomenon is very crucial for reactor safety operation. In this paper, the temperature fluctuations of the lead-based reactor core outlet were simulated by using large eddy simulation (LES) method in the simplified core outlet models. In order to analyze the temperature fluctuation sensitivity for the fuel assembly design parameters, such as the fuel assembly size and the gap between two adjacent fuel assemblies, five geometry models were constructed with different fuel assembly design parameters. The time histories of temperature fluctuations at different monitoring points on the center of three fuel assemblies were obtained. Then the amplitudes and the power spectrum density (PSD) of temperature fluctuations were analyzed, in order to compare temperature fluctuations of different geometry models at the same locations of core outlet. Finally the distribution characteristics of core outlet temperature fluctuations were obtained in axial directions, and the temperature fluctuation sensitivity with fuel assembly parameters was also analyzed based on the amplitudes, PSD and the normalized root-mean square temperature analysis. It is found that the temperature fluctuation intensity is enhanced with the increase of the gap size between adjacent fuel assemblies and the opposite edge width of each fuel assembly. The analysis results could provide important references for optimized design and engineering guidance of lead-based reactor.

1. Introduction

Characterized by excellent materials management capabilities, enhanced safety features and favorable sustainability (Wu, 2016a,b; Wu et al., 2016a,b; GIF website), lead-based reactor has the prospect of achieving industrial demonstration and commercial applications before other Generation IV nuclear reactors concepts according to official evaluation of the Generation IV International Forum (GIF) (Behar et al., 2014).

In a lead-based reactor, when the coolant with different temperature flows out of the reactor core subassemblies, the incompletely mixing of the coolants with different temperatures will lead to a temperature fluctuation. The temperature fluctuation of coolant is transported well to the solid wall of reactor core outlet due to the high thermal conductivity of lead, causing a high cycle thermal fatigue at the solid wall and endangering reactor safety. This phenomenon is called thermal striping (Choi and Kim, 2007). In addition, the amplitude and frequency of the temperature fluctuation are very important parameters that affect the thermal striping phenomenon. And the temperature fluctuation of coolant is the source of thermal fatigue. Thus, studying temperature fluctuation characteristics of core outlet is very important for the reactor core thermal hydraulic optimization design to ensure safety operation of nuclear power plant.

Several numerical studies have been conducted in the past to investigate the temperature fluctuation characteristics of sodium cooled fast reactors as also liquid metal cooled fast reactor. Choi et al. (2015) performed a computational study of thermal striping in the upper plenum of the prototype generation-IV sodium cooled fast reactor (PGSFR), using both of Reynolds-averaged Navier-Stokes (RANS) and large eddy simulation (LES) methods. The study shows that the prediction by the LES gives more appropriate results than that by the k-ε turbulence model. And the amplitude and frequency of the temperature fluctuation at the several locations of the upper internal structure and intermediate heat exchanger were also researched. Lv (2012) simulated the coolant temperature fluctuation from the outlet of the core in China Exper-

* Corresponding author.
E-mail address: guowei.wu@fds.org.cn (G. Wu).

https://doi.org/10.1016/j.anucene.2018.03.020
0306-4549/

imental Fast Reactor (CEFR) using LES method. Transient temperature curves of some typical locations of core outlet were obtained. The results show that the amplitude of temperature fluctuations increases with the increase of vertical height. Furthermore it is found that different fluid conditions only affect the amplitude of temperature fluctuations, almost don't affect the frequency for the measuring points on the same height. Cao (2012) analyzed the characteristics of 3-D temperature fluctuation based on the variations of inlet temperatures, inlet velocities and the cold and hot velocity ratios. For experiment study, the axially symmetric section was designed and 3-D temperatures were measured. For simulation study, Cao et al. (2012) simulated parallel triple-jet flows and coaxial-jet flows by LES and it was shown that the temperature fluctuations were three dimensional in coaxial-jet flows, while those were two dimensional in parallel triple-jet flows.

However, few detailed researches about temperature fluctuation at core outlet of lead-based reactors or thermal striping characteristics for lead-based materials (lead or lead-bismuth) have been done compared with sodium cooled reactors.

Wang et al. (2016a) compared the normalized amplitudes and frequencies of temperature fluctuations of lead, Lead-Bismuth Eutectic (LBE) and sodium in double jet model in order to compare temperature fluctuations of lead-based reactor and that of sodium cooled reactor. It is concluded that both amplitudes and frequencies of lead-based materials fluctuations are larger compared with that of sodium temperature fluctuations. These kinds of studies are valuable because of the availability of limited researches about thermal striping in lead cooled reactors.

In this paper, the core outlet temperature fluctuation of the lead-based reactor was simulated using simplified core outlet model. Moreover, the basic computational model was constructed by referring to Advanced Lead-cooled Fast Reactor European Demonstrator (ALFRED) fuel assembly design (PSI, 2012). To analyze the temperature fluctuation sensitivity with the gap size between two adjacent fuel assemblies and the fuel assembly size, another four geometry models were created with different parameters. Then for the purpose of comparing temperature fluctuations of different locations of core outlet, the amplitudes and the power spectrum density (PSD) of temperature fluctuations were analyzed. Finally the distribution characteristics of core outlet temperature fluctuations were obtained in axial directions. Then the temperature fluctuation sensitivity with fuel assembly parameters was analyzed based on the amplitudes and PSD analysis. The analysis results would provide important design references for instruments arrangement, reactor structure optimization and safety guidance at core outlet and future practical operation of lead-based reactors. In the following sections, calculation model are given, followed by the results and discussion, fuel assembly parameters sensitivity analysis, and some concluding remarks.

2. Calculation model

2.1. Geometry model

In this study, the simplified core outlet model of the lead-based reactor was established as shown in Fig. 1 (Lv, 2012). The temperature fluctuations between fuel assemblies was main concerned about therefore the fuel rod model in the assembly was not constructed. Three fuel assemblies that are adjacent each other were selected and they are arranged as equilateral triangle as shown in Fig. 2. The parameters of fuel assemblies were referenced from ALFRED design and the model with these parameters was set as a basic model for further comparison analysis.

Other geometry models by referencing European Lead cooled Fast Reactor (ELFR) (PSI, 2013) and China LEAd-based Research Reactor (CLEAR-I) (Wu, 2016a,c; Wang et al., 2015a,b) were constructed to obtain the temperature fluctuation sensitivity with the fuel assembly design parameters such as the opposite edge width of each fuel assembly and the gap between two adjacent fuel assemblies shown as H and d in the left of Fig. 2.

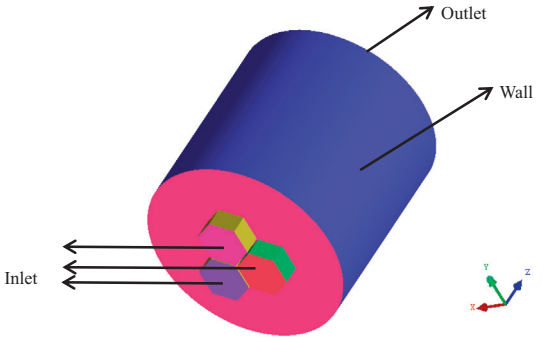

Fig. 1. Computational model.

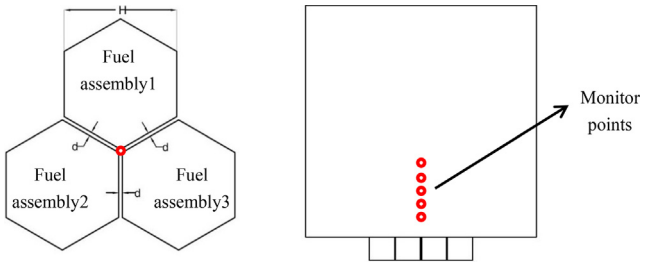

Fig. 2. Monitoring points.

The opposite edge width H of each fuel assembly for respectively case 1, case 2 and case 3 is same while the gap d between adjacent fuel assemblies for respectively case 2, case 4 and case 5 is same. Table 1 summarizes the geometry models with different parameters in this paper.

In addition, in the present study several temperature monitoring points were set at 25 mm, 50 mm, 75 mm, 100 mm and 125 mm respectively from the center of three fuel assemblies in axial direction from core outlet as shown in Fig. 2, respectively.

2.2. Boundary conditions

In the simulation, lead was chosen as the fluid medium and the operating pressure is the ambient pressure (101,325 Pa).

Inlet boundary (ANSYS FLUENT, 2013) conditions were applied at the inlet of the three fuel assemblies for each geometry model.

The inlet velocity of each of the three assemblies for each geometry model was set as 1.4 m/s by referring to ALFRED design (PSI, 2012) and the inlet temperatures were at 765.15 k, 747.15 k and 747.15 k, respectively. The boundary condition input parameters are also summarized in Table 1.

Table 1
Boundary conditions.

Case	Hot inlet		Cold inlet		d (mm)	H (mm)
	Velocity (m/s)	Temperature (K)	Velocity (m/s)	Temperature (K)		
1	1.4	765.15	1.4	747.15	3	166
2					5	166
3					7	166
4					5	120
5					5	204

The inlet boundary conditions are provided by the following equations (Choi et al., 2004; ANSYS FLUENT, 2013):

$$V = V_{in},\ U = W = 0,\ T = T_{in},\ \overline{UV} = \overline{UW} = \overline{VW} = 0 \tag{1}$$

$$\overline{UU} = \overline{VV} = \overline{WW} = \frac{2}{3}K_{in},\ \varepsilon = \varepsilon_{in} \tag{2}$$

$$K_{in} = 1.5(iV_{in})^2,\ \varepsilon_{in} = \frac{C_\mu^{0.75}K_{in}^{1.5}}{D} \tag{3}$$

where i is the turbulence intensity, D is the dissipation length scale. In this paper study we specified D as the hydraulic diameter.

Outflow (ANSYS FLUENT, 2013) boundary conditions were applied at the calculation model exit. And there are the non-slip and adiabatic boundary conditions at the walls.

2.3. Turbulence model

Furthermore, LES turbulence model was applied in the present study considering that many researchers have demonstrated that the numerical results of thermal striping by the LES method are in good agreement with the available experimental data and LES is very appropriate to predict unsteady characteristics of thermal striping (Chacko et al., 2011; Tenchine et al., 2013; Kim et al., 2014; Choi et al., 2004, 2015).

In the LES model, the governing equations for the conservation of mass, momentum, and energy for an incompressible flow can be written as follows (Chacko et al., 2011; Choi et al., 2015):

$$\frac{\partial}{\partial x_i}(\overline{U_i}) = 0 \tag{4}$$

$$\frac{\partial}{\partial t}(\overline{U_i}) + \frac{\partial(\overline{U_iU_j})}{\partial x_j} = -\frac{1}{\rho}\frac{\partial \overline{P}}{\partial x_i} + \frac{\mu}{\rho}\frac{\partial^2 \overline{U_i}}{\partial x_j \partial x_j} - \frac{\partial \tau_{ij}}{\partial x_j} \tag{5}$$

$$\frac{\partial \overline{\Theta}}{\partial t} + \overline{U_i}\frac{\partial \overline{\Theta}}{\partial x_i} = \frac{\partial}{\partial x_i}\left[\left(k + \frac{v_{SGS}}{Pr^{(t)}}\right)\frac{\partial \overline{\Theta}}{\partial x_i}\right] \tag{6}$$

where $\overline{P}$ is the filtered pressure, ρ is the density, $\overline{\Theta}$ is the filtered temperature, k is the molecular diffusivity, v_{SGS} is the SGS eddy viscosity and $Pr^{(t)}$ is subgrid Prandtl number. $\overline{U_i}$ are filtered velocity components such as:

$$\overline{f}(x_i, t) = \iiint_{vol} G(x_i - x_i')f(x_i',\ t)dx_i' \tag{7}$$

The Smagorinsky–Lilly model was used to model the sub-grid scale (SGS) stress tensor (Chacko et al., 2011):

$$\tau_{ij} - \frac{1}{3}\delta_{ij}\tau_{kk} = -2v_{SGS}\overline{S_{ij}} = v_{SGS}\left(\frac{\partial \overline{U_i}}{\partial x_j} + \frac{\partial \overline{U_j}}{\partial x_i}\right) \tag{8}$$

$$v_{SGS} = L_s^2|\overline{S}| = L_s^2\sqrt{(2\overline{S_{ij}S_{ij}})} \tag{9}$$

$$L_s = \min(\kappa d,\ C_s\Delta) \tag{10}$$

where κ is the Kármán constant and d is the distance to the closest wall. Cs is the value of the Smagorinsky constant. The grid filter width is defined as $\Delta = V^{1/3}$, where V is the volume of the computational cell.

2.4. Numerical method

The numerical algorithm employed in the FLUENT code is the PISO algorithm for pressure–velocity coupling. For spatial discretization, a second-order accurate bounded central differencing scheme was used. The second-order upwind scheme was used for turbulence model equations.

The time step was set as 0.001 s referenced by the previous study (Velusamy et al., 2006; Chandran et al., 2010, 2011) and a maximum outer iteration number of 20. Also this time step is small enough to make the Courant number less than 1. What is more, the convergence is declared when the maximum residual of the continuity, momentum and energy equations is less than 0.0001. And the monitoring point temperatures recording was done once per 1 time step.

3. Results and discussion

3.1. Grid sensitivity analysis

In this paper structured hexahedral computational cells were generated by using the ICEM code. And the effect of grid sensitivity analysis was performed based on 3 different grid levels: a coarse grid, a medium grid and a fine grid.

Take case 1 as an example. The average temperatures of the monitoring points are plotted in the Fig. 3. It shows that the results of 10.5 million mesh size differs significantly from 8.6 million mesh size but are consistent and relatively close to that of 12.6 million mesh size. Therefore the 10.5 million mesh size was selected for case 1 considering the computational time and the performance of computers (Wang et al., 2016b). In this way, other cases had been also performed the same grid sensitivity.

3.2. Amplitude and frequency of temperature fluctuation

The amplitudes and the PSD of temperature fluctuations were obtained for 2 s at different monitoring points. The monitoring points positions in the x direction located in X = 0 mm, in the y direction located in Y = 0 mm, while that in the Z direction, located in Z = 25, 50, 75, 100, 125 mm, respectively.

The left of Fig. 4 shows the time histories of temperature fluctuation for case 1 at monitoring points within time = 2 s. It shows that the amplitude of temperature fluctuation is distributed from 748 K to 757 K. And the peak-to-peak value is gradually increasing from 4 K to 9 K while the monitoring location from Z = 25 mm to Z = 125 mm. That means the amplitude of temperature fluctuation increases with the increase of the height from the core outlet for case 1.

The right of Fig. 4 presents that the frequencies primarily distribute below 40 Hz, and the maximum prominent frequency is not obvious at Z = 25 mm while the prominent frequencies are around 7 Hz, 19 Hz, 29 Hz at Z = 50 mm. It is noted that the promi-

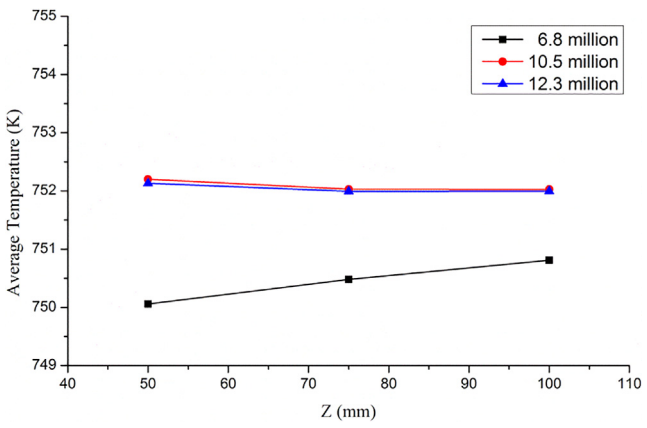

Fig. 3. Grid sensitivity analysis of case 1.

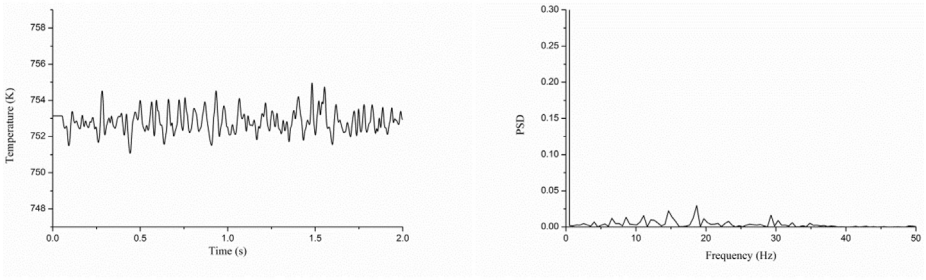

(a) Z=25mm

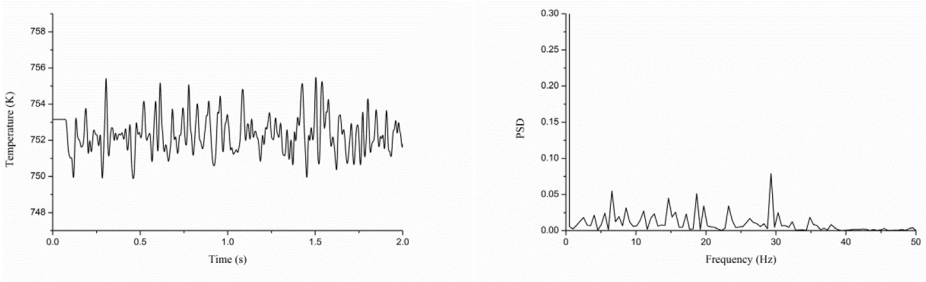

(b) Z=50mm

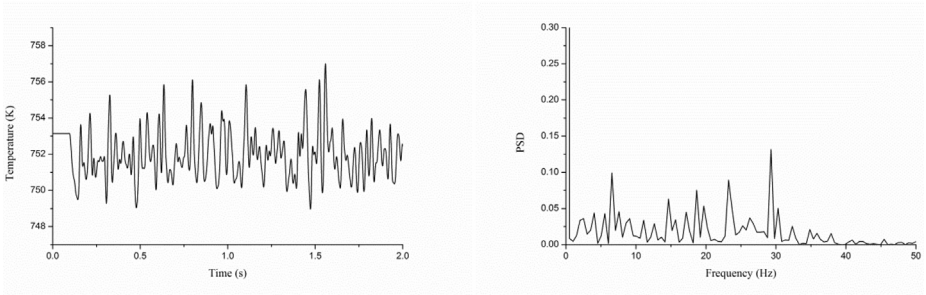

(c) Z=75mm

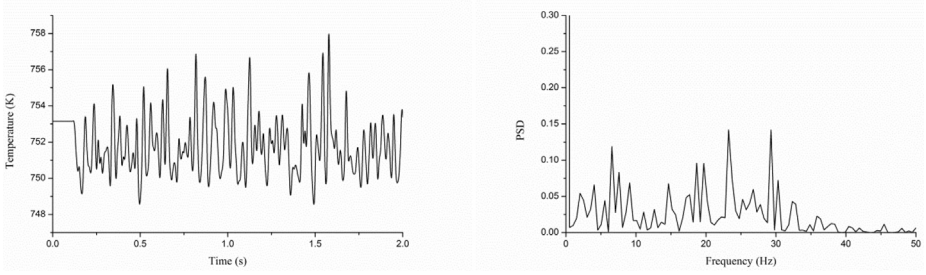

(d) Z=100mm

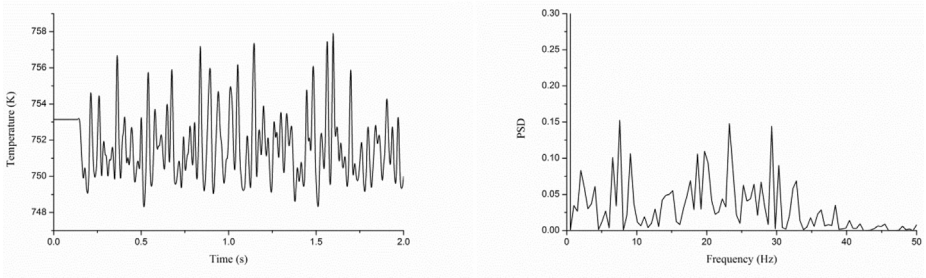

(e) Z=125mm

Fig. 4. Temperature fluctuation of case 1.

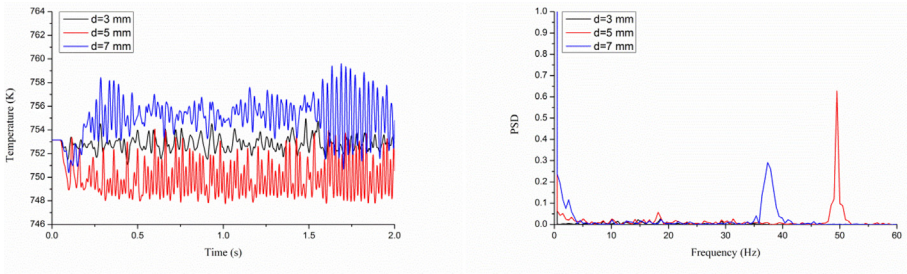

(a) Z=25mm

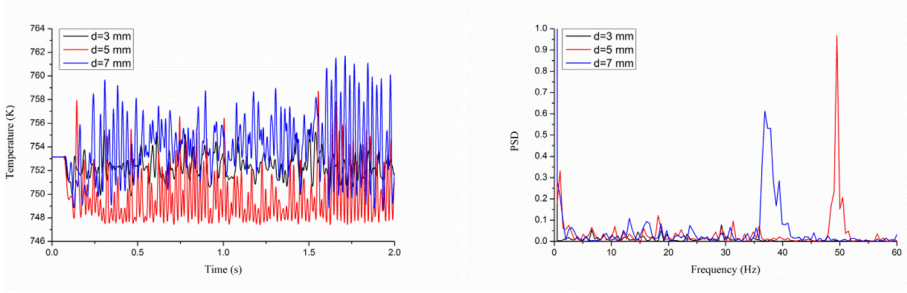

(b) Z=50mm

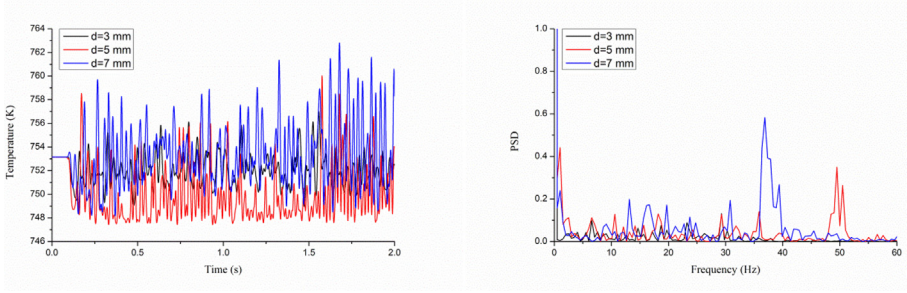

(c) Z=75mm

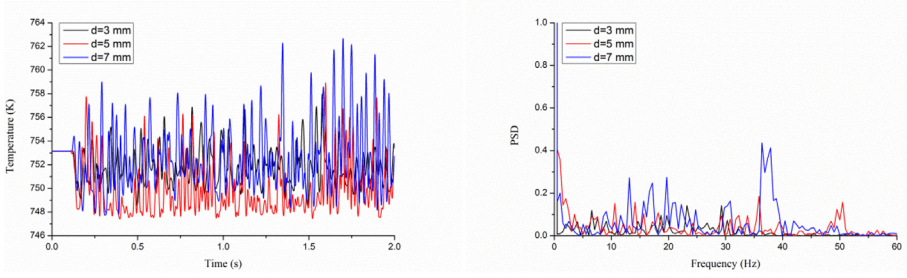

(d) Z=100mm

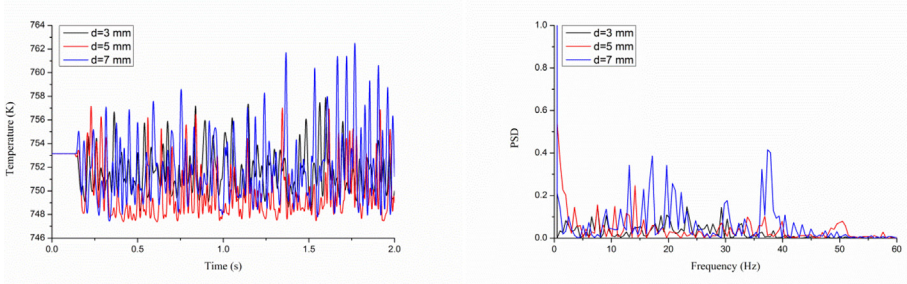

(e) Z=125mm

Fig. 5. Comparison of temperature fluctuation of case 1, case 2 and case 3.

nent frequencies distribution increase at Z = 75 mm, Z = 100 mm and Z = 125 mm when the prominent frequencies are mainly around 7 Hz, 23 Hz, 29 Hz. Therefore the temperature fluctuation intensity increases at central locations along the axial direction in accordance with the prominent frequency distribution characteristics for case 1.

4. Fuel assembly parameters sensitivity analysis

4.1. Effect on temperature fluctuation with d

Fig. 5 shows the time histories of PSD temperature fluctuation for case 1, case 2 and case 3 at Z = 25 mm, 50 mm, 75 mm, 100 mm and 125 mm on the center of three fuel assemblies. It is observed that the amplitude of temperature fluctuation is obviously different for different cases and the peak to peak value of temperature fluctuation for case 3 is maximum one while that of case 1 is minimum one as shown in the left of Fig. 5.

As for the frequency of temperature fluctuation, the frequency distribution and the prominent frequency of different cases are obviously different.

In Z = 25 mm and Z = 50 mm conditions, the right of Fig. 5(a) and (b) show that the prominent frequencies of case 2 and case 3 are very clear which are mainly around 49 Hz and 37 Hz. While compared with case 2 and case 3, the prominent frequency of case 1 is not very obvious. At Z = 75 mm the prominent frequencies of case 2 are about 1 Hz and 49 Hz and the prominent frequency of case 3 is still about 37 Hz as shown in the right of Fig. 5(c). However, in Z = 100 mm condition, the prominent frequencies of case 2 and case 3 distribute on more frequency regions. The prominent frequencies of case 2 are 2 Hz, 11 Hz, 14 Hz, 36 Hz and 49 Hz while the prominent frequencies of case 3 are 13 Hz, 17 Hz, 19 Hz and 37 Hz as shown in the right of Fig. 5(d). In Z = 125 mm condition, the prominent frequencies of case 2 are 4 Hz, 7 Hz, 11 Hz, and 13 Hz when the prominent frequencies of case 3 are 17 Hz, 19 Hz, 36 Hz and 37 Hz as shown in the right of Fig. 5(e). It is noted that the maximum prominent frequency is increasing as the increasing of the d value at Z = 125 mm but the frequency of temperature fluctuation shows no obvious effect with the d value at other locations such as from Z = 25 mm to Z = 100 mm.

To further analyze the effect on temperature fluctuation with the gap d between adjacent fuel assemblies, the normalized root-mean square (RMS) of the instantaneous temperature for 2 s were compared corresponding to different cases.

T^*_{RMS} are defined as (Lu et al., 2010):

$$\overline{T^*} = \frac{1}{N}\sum_{n=1}^{N} T^*_n \tag{11}$$

$$T^*_{RMS} = \sqrt{\frac{1}{N}\sum_{n=1}^{N}\left(T^*_n - \overline{T^*}\right)} \tag{12}$$

where N is the total number of sampling monitoring points. T^*_n is normalized temperature given as:

$$T^*_n = \frac{T_n - T_c}{T_h - T_c} \tag{13}$$

where T_n is the instantaneous temperature at a given location, T_c is the cold fluid inlet temperature, and T_h is the hot fluid inlet temperature.

Fig. 6 presents the T^*_{RMS} at different monitoring points of case 1, case 2 and case 3 for 2 s. It indicates the T^*_{RMS} is increasing with the increase of the d value. In other words with the increase of the gap between adjacent fuel assemblies the temperature fluctuation intensity is slightly enhanced for 2 s from Z = 25 mm to Z = 125 mm. Meanwhile, it is inferred that because the space of hot and cold fluid mixing is increasing as the increasing of the gap between adjacent fuel assemblies, the temperature fluctuation intensity is enhanced with the increase of the gap size between adjacent fuel assemblies. However, the temperature fluctuation will disappear when the gap size between adjacent fuel assemblies is infinitely far away. Therefore, there may be a special gap size which make the temperature fluctuate most strongly.

4.2. Effect on temperature fluctuation with H

Fig. 7 shows the time histories and the PSD of temperature fluctuation for case 2, case 4 and case 5 at Z = 25 mm, 50 mm, 75 mm, 100 mm and 125 mm at the center of three fuel assemblies. It is observed that the peak to peak value of temperature fluctuation for case 5 is maximum compared with that of case 2 and case 4. It means that the amplitude of temperature fluctuation is higher with bigger H value from Z = 25 mm to 125 mm location as shown in the left of Fig. 7.

As for the frequency of temperature fluctuation, the maximum prominent frequency shows change law with the H value from Z = 25 mm to Z = 100 mm. In Z = 25 mm and Z = 50 mm condition, the maximum prominent frequency of case 2, case 4 and case 5 is 1 Hz, 49 Hz and 51 Hz as shown in the right of Fig. 7(a) and (b). In Z = 75 mm condition, the maximum prominent frequency of case 5 is 51 Hz while the maximum prominent frequency of case 2 and that of case 4 are same as shown in the right of Fig. 7(c). However, the submaximal prominent frequency 49 Hz of case 2 is higher than that of 3 Hz of case 4. Furthermore, Fig. 7(d) shows that the maximum prominent frequency of case 2, case 4 and case 5 is 1 Hz, 2 Hz and 51 Hz. Thus with the increase of the opposite edge width H of each fuel assembly the maximum prominent frequency of temperature fluctuation is increasing from Z = 25 mm to Z = 100 mm for 2 s. But at Z = 125 mm the maximum prominent frequency of case 2, case 4 and case 5 is 1 Hz, 7 Hz and 14 Hz as shown in Fig. 7(e). It means that the frequency of temperature fluctuation shows no obvious effect with the H value at Z = 125 mm.

Fig. 8 presents the T^*_{RMS} at different monitoring points of case 2, case 4 and case 5 for 2 s. It shows that the T^*_{RMS} is increasing with the increase of H value. It means that with the increase of the opposite edge width H of each fuel assembly the temperature fluctuation intensity is enhanced for 2 s from Z = 25 mm to 125 mm. As a result of that the mass flowrate is increasing as the increasing of H when the inlet velocity is constant, the temperature fluctuation intensity is enhanced with the opposite edge width H of each fuel assembly.

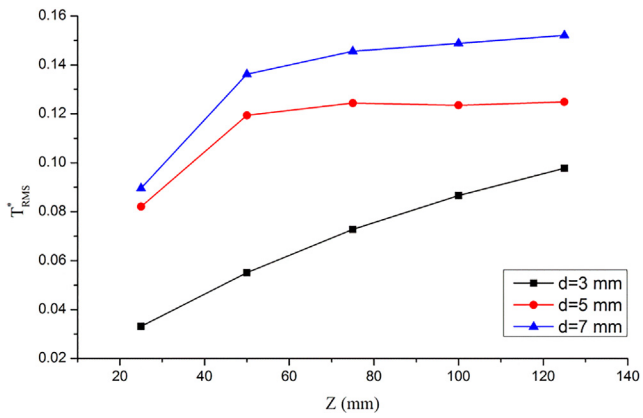

Fig. 6. The RMS temperature of case 1, case 2 and case 3.

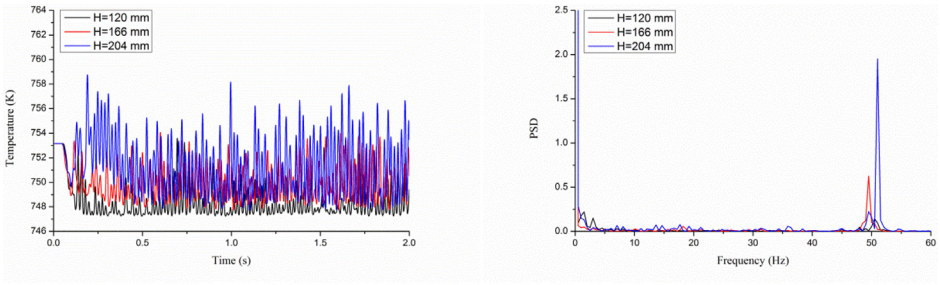

(a) Z=25mm

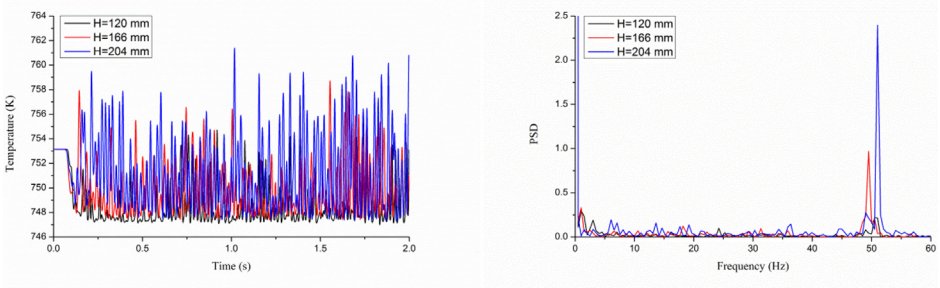

(b) Z=50mm

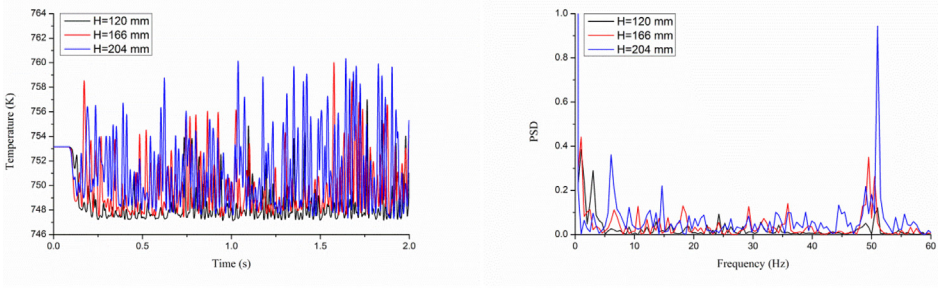

(c) Z=75mm

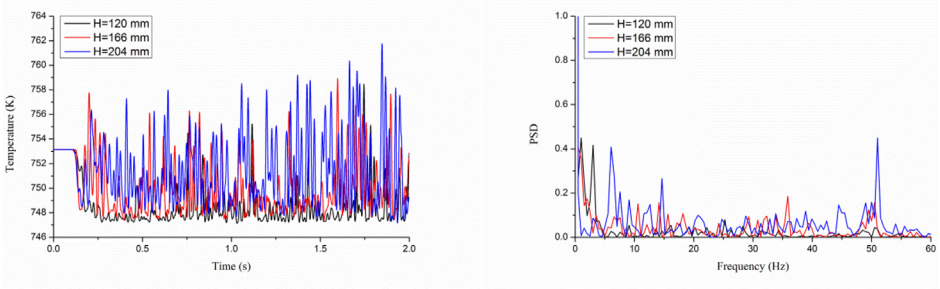

(d) Z=100mm

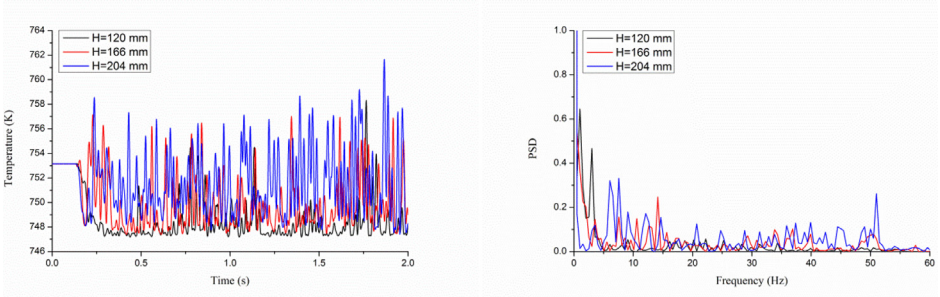

(e) Z=125mm

Fig. 7. Comparison of temperature fluctuation of case 2, case 4 and case 5.

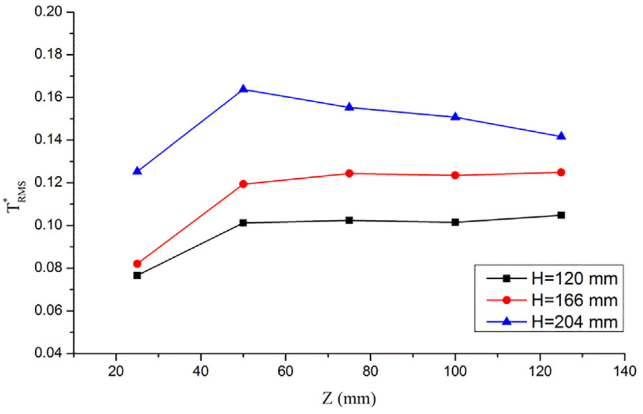

Fig. 8. The RMS temperature of case 2, case 4 and case 5.

Furthermore, it is found that the case 5 shows different T^*_{RMS} dependence on Z with case 2 and case 4. The T^*_{RMS} of case 5 is increasing with the increase of Z from Z = 25 mm to 50 mm, while decreasing with the increase of Z from Z = 50 mm to 125 mm. However, the T^*_{RMS} of case 2 and case 4 is increasing with the increase of Z from Z = 25 mm to 50 mm and then nearly remaining stable from Z = 50 mm to 125 mm. The difference may be induced by the larger opposite edge width H of each fuel assembly for case 5. When the inlet velocity is same, the mass flowrate of case 5 is larger than other cases. Thus, it is easier for case 5 to reach the maxim T^*_{RMS} when the Z value is very small. Meanwhile, the flowing and mixing is becoming complete as the increasing of the Z value and then the T^*_{RMS} is showing decreasing tendency but still larger than that of case 2 and case 4.

5. Conclusions

Numerical investigations of the coolant temperature fluctuation for the lead-based reactor core outlet were performed. In order to study the temperature fluctuation sensitivity with the fuel assembly design parameters, the amplitude and PSD of temperature fluctuations by 5 simplified core outlet models of the lead-based reactor with monitoring points from Z = 25 mm to 125 mm on the center of three fuel assemblies for 2 s were analyzed. The following conclusions were drawn from the results:

(1) When the opposite edge width H of each fuel assembly is same, the amplitude peak to peak value of temperature fluctuation is increasing with the increase of the gap d between adjacent fuel assemblies, while the frequency shows no obvious effect with the d value. Moreover, the temperature fluctuation intensity is slightly enhanced from view of the RMS temperature for 2 s from Z = 25 mm to Z = 125 mm.
(2) When the gap d keeps constant, with the increase of the opposite edge width H of each fuel assembly, the amplitude peak to peak value of temperature fluctuation is increasing and the maximum prominent frequency of temperature fluctuation is increasing from Z = 25 mm to Z = 100 mm. Furthermore, the temperature fluctuation intensity is enhanced from view of the RMS temperature for 2 s from Z = 25 mm to Z = 125 mm.

The effect on temperature fluctuation of the lead-based reactor core outlet with the thermal hydraulic parameters will be performed such as temperature differences, velocity ratio in simplified model with more fuel assemblies in the future.

Acknowledgements

This work was supported by Natural Science Foundation of Anhui Province of China (Grant No. 1608085ME107). The authors are grateful to other members of FDS Team for their great help in this research.

References

ANSYS FLUENT 13.0 User's Guide, 2013.
Behar, C. et al., 2014. Technology roadmap update for generation IV nuclear energy system. OECD Nuclear Energy Agency for the Generation IV International Forum.
Cao, Q., 2012. Research on the 3-D Coolant Temperature Fluctuation in Upper Plenum of the Core in Nuclear Reactor (Thesis for the Doctoral Degree in Engineering of North China). Electric Power University.
Cao, Q., Lu, D., Lv, J., 2012. Numerical investigation on temperature fluctuation of the parallel triple-jet. Nucl. Eng. Des. 249, 82–89.
Chacko, S., Chung, Y.M., Choi, S.K., 2011. Large eddy simulation of thermal striping in unsteady no-isothermal triple jet. Int. J. Heat Mass Transf. 54, 4400–4409.
Chandran, R.K., Banerjee, I., Padmakumar, G., et al., 2010. Numerical analysis of thermal striping phenomena using a two jet water model. Eng. Appl. Comput. Fluid. 4 (2), 209–221.
Chandran, R.K., Banerjee, I., Padmakumar, G., et al., 2011. Investigation of thermal striping in prototype fast breeder reactor using ten-jet water model. Heat Transf. Eng. 32 (5), 369–383.
Choi, S.K., Kim, D.E., Ko, S.H., et al., 2015. Large eddy simulation of thermal striping in the upper plenum of the PGSFR. J. Nucl. Sci. Technol. 52 (6), 878–886.
Choi, S.K., Kim, S.O., 2007. Evaluation of turbulence models for thermal striping in a triple jet. J. Pressure Vessel Technol. 129, 583–592.
Choi, S.K., Kim, E.K., Wl, M.-H., et al., 2004. A numerical simulation of thermal striping in an upper plenum of a liquid metal reactor. ASME/JSME Pressure Vessels & Piping Conference.
Generation IV International Forum. Lead-Cooled Fast Reactor (LFR). https://www.gen-4.org/gif/jcms/c_42149/lead-cooled-fast-reactor-lfr.
Kim, D.E., Ko, S.H., Jeno, W.D., et al., 2014. Computation of thermal striping in the upper plenum of PGSFR. In: Proceedings of the 2014 22nd International Conference of Nuclear Engineering, pp. 1–6.
Lu, T., Jiang, P.X., Guo, Z.J., et al., 2010. Large-eddy simulations (LES) of temperature fluctuations in a mixing tee with/without a porous medium. Int. J. Heat Mass Transf. 53 (21), 4458–4466.
Lv, J., 2012. Numerical Simulation on Coolant Temperature Fluctuation from the Outlet of The Core in China Experimental Fast Reactor (Thesis for the Master Degree of North China). Electric Power University.
PSI, 2012. LEADER WP2, Thermal-hydraulic Assessment of the ETDR Core.
PSI, 2013. LEADER WP2, Thermal-hydraulic Assessment of the ELFR Core.
Tenchine, D., Vandroux, S., Barthel, V., et al., 2013. Experimental and numerical studies on mixing jets for sodium cooled fast reactors. Nucl. Eng. Des. 263, 263–272.
Velusamy, K., Natesan, K., Selvaraj, P., et al., 2006. CFD studies in the prediction of thermal striping in an LMFBR. In: CFD4NRS Conference, Garching, Munich, Germany.
Wang, L., Bai, Y., Jin, M., et al., 2016a. Comparison analysis of temperature fluctuations for double jet of liquid metal cooled fast reactor. Ann. Nucl. Energy 94, 802–807.
Wang, M., Huang, H., Lian, C., et al., 2015a. Conceptual design of lead cooled reactor for hydrogen production. Int. J. Hydrogen Energy 40, 15127–15131.
Wang, M., Lian, C., Li, Y., et al., 2015b. Preliminary conceptual design of a lead-bismuth cooled small reactor (CLEAR-SR). Int. J. Hydrogen Energy 40, 15132–15136.
Wang, X., Jin, M., Wu, G., et al., 2016b. Natural circulation characteristics of lead-based reactor under long-term decay heat removal. Prog. Nucl. Energy 90, 11–18.
Wu, Y., 2016a. CLEAR-S: an integrated non-nuclear test facility for China lead-based research reactor. Int. J. Energy Res. 40 (14), 1951–1956.
Wu, Y., 2016b. Development of high intensity D-T fusion neutron generator HINEG. Int. J. Energy Res.
Wu, Y., 2016c. Design and R&D progress of China lead-based reactor for ADS research facility. Engineering 2 (1), 124–131.
Wu, Y., Bai, Y., Song, Y., et al., 2016a. Development strategy and conceptual design of china lead-based research reactor. Ann. Nucl. Energy 87, 511–516.
Wu, Y., Chen, Z., Hu, L., et al., 2016b. Identification of safety gaps for fusion demonstration reactors. Nat. Energy 1, 16154.